Available online at www.sciencedirect.com
SCIENCE DIRECT®
Journal of Molecular Catalysis A: Chemical 217 (2004) 219–229
JOURNAL OF MOLECULAR CATALYSIS A: CHEMICAL
www.elsevier.com/locate/molcata

Hydrogenation of hexanal over sulfided Ni-Mo/γ-Al_2O_3 catalysts

Xueqin Wang, Gongliang Li, Umit S. Ozkan*

Department of Chemical Engineering, The Ohio State University, 140 West 19th Avenue, Columbus, OH 43210, USA

Received 27 December 2003; received in revised form 27 March 2004; accepted 27 March 2004

Abstract

Hydrogenation of hexanal to hexanol was studied over sulfided Ni-Mo catalysts supported on γ-Al_2O_3. Characterizations of the oxide and sulfide forms of the catalysts were performed using XRD, XPS, TPD, DRIFTS, and TEM/EDX techniques. The relationship between the molybdena surface coverage and the density of surface hydroxyl groups and their correlation with CO_2 adsorption sites have been investigated. A strong correlation was observed between the selectivity of the catalysts towards heavy products, such as dimers, trimers and acetals and CO_2 adsorption sites. The water resistance of the catalyst was also examined by keeping the catalyst on stream for 300 h. Post-reaction characterization of the catalysts performed using XPS technique showed partial oxidation of Mo sites and preferential loss of Ni from the surface.

Keywords: Hexanal hydrogenation; Sulfided Ni-Mo catalysts; Water tolerance; XPS; TEM; DRIFTS; XRD; Hydroxyl groups

1. Introduction

As the primary catalysts used for hydrotreating processes, sulfided molybdenum and tungsten catalysts have been studied extensively [1–7]. Hydrodesulfurization (HDS) and hydrodenitrogenation (HDN) are the primary catalytic hydrotreating processes that have been investigated extensively because of the environmental concerns associated with the combustion of organonitrogen and organosulfur compounds and because these type of compounds are the major impurities in traditional petroleum feedstocks. HDS and HDN studies have led to a good understanding of the mechanisms involved in these reactions and effective catalysts have been developed for these two processes. The major catalysts used for HDS and HDN are sulfided CoMo and NiMo catalysts that are supported on Al_2O_3. According to a widely accepted model proposed by Topsoe and co-workers, these catalysts consist of stacks of MoS_2 layers supported over alumina and the Ni or Co species are located on the edges of these stacks (i.e., CoMoS and NiMoS phases) [3,8–10].

Oxo process alcohols are a major class of organic chemicals [11]. The oxo process (i.e., hydroformylation) consists of reacting an olefin with carbon monoxide and hydrogen at elevated temperatures and pressures, in the presence of a suitable catalyst, to produce an aldehyde with a carbon number one higher than the starting olefin. However, the homogeneous catalysts in the hydroformylation reaction are not effective for hydrogenation catalysis; thus, further hydrogenation is required in a separate reactor. A wide range of heterogeneous catalysts is used in the industry to convert aldehydes to alcohols. Catalysts frequently used include copper chromite, molybdenum sulfide, nickel, and cobalt. However, copper chromite is very sensitive to sulfur compounds. Sulfided Ni-Mo catalysts provide high hydrogenation activity as well as high tolerance to sulfur [12,13].

Although there is ample literature on the application of sulfided Ni-Mo catalysts in hydrotreating and especially in HDN reactions, there have not been many studies focusing on their application in aldehyde hydrogenation reactions. Especially an understanding of how the surface characteristics correlate with different reaction pathways is lacking. In a series of papers, we present the results from our recent investigations on the catalytic performance of sulfided Ni-Mo/γ-Al_2O_3 catalysts in hydrogenation of lower aldehydes and their pre- and post-reaction, and in situ characterization using BET, XRD, TEM, XPS, and DRIFTS techniques.

* Corresponding author. Tel.: +1-614-292-6623; fax: +1-614-292-9615.
E-mail address: ozkan.1@osu.edu (U.S. Ozkan).

1381-1169/$ – see front matter © 2004 Elsevier B.V. All rights reserved.
doi:10.1016/j.molcata.2004.03.037

2. Experimental

2.1. Catalyst preparation

Alumina-supported catalysts with different MoO_3 and NiO loadings were prepared by wet co-impregnation of γ-Al_2O_3 (Harshaw-Filtre) with aqueous solutions of ammonium heptamolybdate [$(NH_4)_6Mo_7O_{24}{\cdot}4H_2O$] (Fisher) and nickel nitrate [$Ni(NO_3)_2{\cdot}6H_2O$] (Mallinckrodt). The preparation procedure was reported previously [14,15]. Impregnation was carried out at a pH of 8 and a temperature of 60 °C. The slurry was then dried at 60 °C under vacuum followed by drying in a drying oven over night at 110 °C. The resulting powder was calcined at 500 °C under a continuous flow of pure oxygen. The catalyst compositions are reported as weight percentages of the oxide precursors, i.e., MoO_3, NiO, following the convention commonly used in the literature. Prior to all reactions, the catalysts were heated to 400 °C with He and sulfided in situ at 400 °C under a flow of 10% H_2S in H_2 for 10 h, followed by He flushing at the same temperature for 2 h and cooling to reaction temperature.

2.2. Catalyst characterization

The surface areas of oxidic samples calcined at 500 °C in O_2 were measured using BET method with a Micromeritics AccuSorb 2100E instrument, using nitrogen as adsorbent at liquid nitrogen temperature (77 K). The samples were degassed at 125 °C for 12 h before surface area measurements. The properties of oxidic samples were also studied with X-ray powder diffraction (XRD) patterns. The powder diffraction patterns were obtained using a Scintag PAD-V diffractometer with Cu Kα radiation ($\lambda = 1.5432$ Å) as the X-ray source. The diffractometer was operated at 45 kV and 20 mA. The powder diffraction patterns were recorded in the 2θ range from 20 to 80°. The scan rate was set at 1°/min. The diffraction lines were identified by matching experimental patterns to the standard diffraction patterns from 1998 JCPDS database.

Diffuse Reflectance Infrared Fourier Transform Spectroscopy (DRIFTS) experiments were performed using a Bruker IFS66 instrument equipped with a DTGS detector and a KBr beamsplitter. Catalyst was placed in a sample cup inside a Spectratech diffuse reflectance cell equipped with KBr windows and a thermocouple mount that allowed direct measurement of the surface temperature. Spectra for each experiment were averaged over 1000 scans in the mid-IR range (400–4000 cm^{-1}) to a nominal 3 cm^{-1} resolution. After in situ pretreatment of the samples at 400 °C for 2 h in a He flow of 30 cm^3/min, the temperature was decreased to room temperature and the background spectra were taken under He flow. CO_2 adsorption experiments were performed by introducing CO_2 in He gases at a flow rate of 20 cm^3/min into the system at room temperature for 1 h. After adsorption, the system was subsequently purged for 1 h under He of 30 cm^3/min. Then the spectra were collected under He flow and the background spectrum was subtracted from the post-adsorption spectra.

TPD experiments were performed using a built-in-house apparatus, which was previously described [16]. The reactor effluent composition was continually monitored as a function of sample temperature by a mass spectrometer (Hewlett-Packard, MS Engine 5890A). For each of the TPD experiments, 200 mg of sample was loaded in the U-tube quartz reactor. All samples were sulfided in situ using the same procedure as in reaction studies, i.e., flowing 10% H_2S in H_2 for 10 h at 400 °C. CO_2 adsorption experiments were performed by flowing 6.5% CO_2 in He (53.5 cm^3 (STP)/min) into the reactor at 30 °C for 1 h. After being flushed with He for 1 h at the same temperature, the samples were heated up to 600 °C at a rate of 10 °C/min under a 50 cm^3 (STP)/min He flow and the effluent were monitored by the mass spectrometer.

The transmission electron microscope used in this study was Philips CM-300FEG Ultra-Twin FEG TEM with light element energy dispersive X-ray analysis. It is operated at 300 kV accelerating voltage with a high brightness field emission electron gun (FEG) and a 1.7 Å point-to-point resolution.

X-ray photoelectron spectroscopy analysis was performed using V.G.ESCALAB Mark II, operated at 14 kV and 20 mA with Mg Kα radiation (1253.6 eV). Binding energies were referenced to Al 2p of 74.4 eV.

XPS and TEM/EDX analyses on sulfided and post-reaction catalysts were done without exposing samples to the atmosphere. Catalysts were flushed with He at 400 °C for 2 h after sulfidation or reaction and then cooled to room temperature under He flow. The samples were then sealed using the valves located at both ends of the reactor tube. The reactors were then taken to an argon-atmosphere glove box, where the catalysts were removed and mounted on the XPS and TEM sample holders. The samples were then transferred to the XPS or TEM chamber without exposure to air.

2.3. Reaction studies

Hydrogenation of hexanal was carried out in a fixed bed flow reactor, which made out of 1/4 in.(4.6 mm) (i.d.) stainless steel tubing. The reactor had two isolation valves on each end to allow its removal from the reaction system and air-free transfer for post-reaction characterization. The amount of catalyst loaded into the reactor corresponded to a total surface area of 25 m^2 except when otherwise noted. Reaction temperatures were in the range of 140–180 °C and pressure was kept at 1000 psig (6.9×10^6 Pa) for all runs and was controlled by a backpressure regulator (Tescom 26-1723). The gas flow rates were controlled by Mass Flow Controllers (Brooks instrument, 5850TR). Hexanal and other feeds were introduced into the reaction system by either saturating a stream in H_2 using a bubbler or pumping with Eldex M2.0

syringe pump. The concentration of feed was controlled by the temperature of bubbler or pump meter and verified by GC analysis. The outlet of reactor was connected directly to a condenser, which was cooled in an ice-water bath. Decane was used as the solvent in the condenser. The outlet flow was switched to the condenser after reaction reached steady state. Condensed species were analyzed by GC using the auto liquid injector. The lighter components were analyzed on-line using the gas injection mode of the GC.

3. Results and discussion

3.1. Characterization of oxide samples

3.1.1. BET and XRD studies

The surface area of samples used in these studies varied between 167 and 195 m^2/g, with pure alumina giving the highest surface area (Table 1). The surface area of MoO_3/γ-Al_2O_3 samples decreased gradually with MoO_3 loading up to 15%, but showed a more pronounced decrease when MoO_3 loading increased to 20%. There was no significant effect of NiO addition on the surface area of 15% MoO_3/γ-Al_2O_3 at lower loading levels (<5%), while a pronounced decrease of surface area was observed for higher loadings (7%).

The X-ray diffraction patterns of γ-Al_2O_3 support and the mono-metallic oxidic samples are presented in Fig. 1. X-ray diffraction patterns of the monometallic samples (Fig. 1(I)) with MoO_3 loading levels lower than 15% show no noticeable difference from that of γ-Al_2O_3 matrix, except for a slight decrease in peak intensity at a *d*-spacing of 1.40 Å (4 4 0), 1.98 Å (4 0 0), and 2.33 Å (3 1 1) corresponding to γ-Al_2O_3 phase. X-ray diffraction pattern of oxidic monometallic sample with 15% loading presents the evidence of a new crystalline phase emerging, even though it is not pronounced. It is consistent with the laser Raman spectroscopy results reported earlier [15] where evidence of three-dimensional MoO_3 domains were visible at loading levels of 15 % or above. When MoO_3 loading reaches 20%, the diffraction lines from crystalline MoO_3 at *d*-spacing of 3.810 Å (1 1 0), 3.463 Å (0 4 0) and 3.260 Å (0 2 1) appear much more strongly and the intensity increases with loading

Table 1
BET surface area of oxidic samples

Sample	Surface area (m^2/g)
γ-Al_2O_3	195
4% MoO_3/γ-Al_2O_3	192
10% MoO_3/γ-Al_2O_3	187
15% MoO_3/γ-Al_2O_3	183
20% MoO_3/γ-Al_2O_3	168
15% MoO_3-1% NiO/γ-Al_2O_3	184
15% MoO_3-3% NiO/γ-Al_2O_3	184
15% MoO_3-5% NiO/γ-Al_2O_3	181
15% MoO_3-7% NiO/γ-Al_2O_3	167

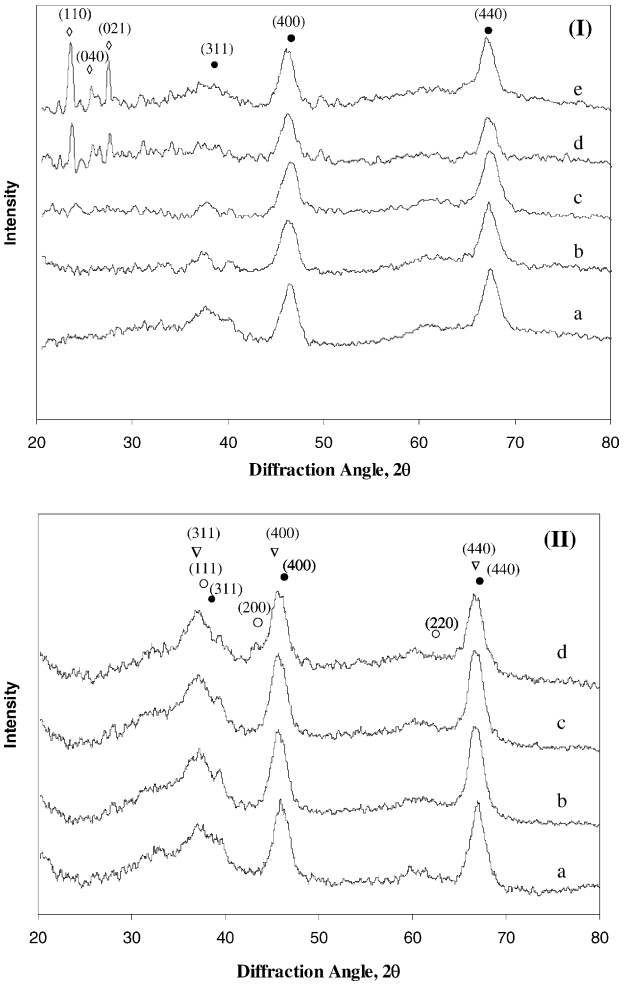

Fig. 1. X-ray diffraction patterns of oxidic mono-metallic catalysts: (●) γ-alumina, (◇) molybdenum trioxide, (▽) nickel aluminate, (○) nickel oxide. (I): (a) 4% MoO_3/γ-Al_2O_3, (b) 10% MoO_3/γ-Al_2O_3, (c) 15% MoO_3/γ-Al_2O_3, (d) 20% MoO_3/γ-Al_2O_3, (e) 25% MoO_3/γ-Al_2O_3. (II): (a) γ-Al_2O_3, (b) 3% NiO/γ-Al_2O_3, (c) 5% NiO/γ-Al_2O_3, (d) 7% NiO/γ-Al_2O_3.

up to 25%. Fig. 1(II) shows the X-ray diffraction patterns of oxidic monometallic samples with different NiO loadings over Al_2O_3 surface. With increasing Ni loading, the diffraction lines that correspond to γ-Al_2O_3 phase shift towards lower angles and become broader. One possible explanation of this shift may be the formation of $NiAl_2O_4$, which has a (3 1 1) *d*-spacing of 2.41 Å. A distinct diffraction line of crystalline NiO at *d*-spacing of 2.09 Å (2 0 0) was identified when Ni loading reached to 7%. Fig. 2 shows the X-ray diffraction patterns of bi-metallic Ni-Mo samples. Comparing diffraction patterns of bi-metallic Ni-Mo samples with mono-metallic Mo samples, it can be seen that the intensity of the peaks corresponding to γ-Al_2O_3 phase decreases with Ni addition. No apparent lines from MoO_3 crystalline phase are observed over the bi-metallic catalyst. Below 5% NiO loading, the diffraction lines that correspond to $NiAl_2O_4$ and crystalline NiO phases are not present. With increasing Ni loading, new features appear at d-spacing of

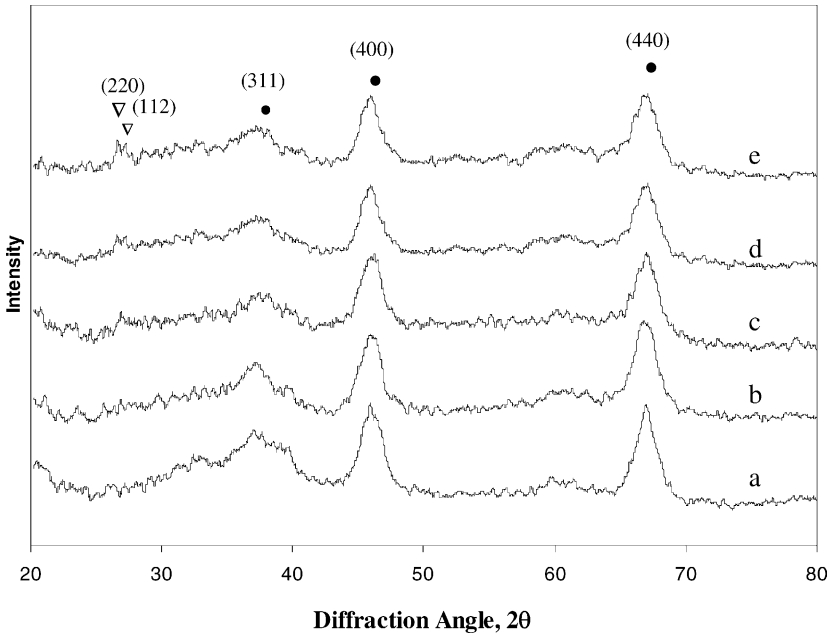

Fig. 2. X-ray diffraction patterns of bi-metallic samples: (●) γ-alumina, (▽) nickel molybdate. (a) γ-Al_2O_3, (b) 1% Ni-15% Mo/γ-Al_2O_3, (c) 3% Ni-15% Mo/γ-Al_2O_3, (d) 5% Ni-15% Mo/γ-Al_2O_3, (e) 7% Ni-15% Mo/γ-Al_2O_3.

3.35 and 3.28 Å, which can be assigned to (2 2 0) and (1 1 2) diffraction lines of β-$NiMoO_4$ (JCPDS—45-0142, 1988). Presence of nickel molybdate on sulfided Ni-Mo catalysts was reported previously [17, 18, and references therein, 19]. Some authors characterized the nickel molybdate in these samples as $xNiO{\cdot}MoO_3{\cdot}yH_2O$, while others reported a metastable β-$NiMoO_4$ phase.

3.1.2. DRIFTS spectra of oxide samples

IR studies of surface OH groups on MoO_3/γ-Al_2O_3 catalysts are considered to provide important insight into the interaction between molybdenum species and alumina surface. Our studies have also shown different OH groups on bare γ-Al_2O_3 surfaces to play an important role in the reaction network of aldehyde hydrogenation. Five types of OH groups on the surface of γ-Al_2O_3 are reported [20], ranging from the basic terminal OH species, coordinated to a single tetrahedral Al^{3+}, to the acidic bridging OH groups coordinated to three Al^{3+} cations in octahedral interstices. The surface OH groups are easily distinguished by the IR technique. The bands assigned to the more basic hydroxyls appear to be located at higher wavenumbers. The increase in acidity of a hydroxyl group shifts the corresponding band to lower wavenumbers.

The hydroxyl regions of the IR spectra of γ-Al_2O_3 and MoO_3/γ-Al_2O_3 samples studied by DRIFTS technique are shown in Fig. 3(a). Over γ-Al_2O_3 surface, well-defined OH bands at 3675 and 3728 cm^{-1} and a small shoulder band at 3769 cm^{-1} are observed together with unresolved bands at around 3748 and 3785 cm^{-1}, in agreement with previous reports [21,22]. The broad and intense band centered at about 3580 cm^{-1} in each spectrum is indicative of H-bonded hydroxyls. The bands at higher wavenumbers (3748, 3769, and 3785 cm^{-1}), which correspond to more basic OH groups, disappear preferentially at lower Mo loadings. Hydroxyl groups at lower frequencies (3728 and 3675 cm^{-1}) are eliminated gradually with further increase in Mo loading. The inset figure shows the IR spectra of MoO_3/Al_2O_3 samples after subtraction of the bare Al_2O_3 support spectrum. The negative peaks correspond to OH groups used in "anchoring" molybdena species. This observation is consistent with earlier findings [21,23,24] in that Mo species interact favorably with the more basic surface hydroxyl groups of alumina. All hydroxyl bands except the one at 3785 cm^{-1} disappear at MoO_3 loading exceeding monolayer coverage (about 15%). The band at 3785 cm^{-1} was not eliminated completely until 25% MoO_3 loading level is reached. It is conceivable that these hydroxyl groups are less easily accessible to molybdena complexes in the precipitation medium.

After the IR spectra of freshly pretreated γ-Al_2O_3 and MoO_3/γ-Al_2O_3 series of samples were recorded, CO_2 was introduced into the chamber at room temperature, followed by desorption of weakly held CO_2 at room temperature by He flushing. The IR spectra of the OH region are recorded and shown in Fig. 3(b). Comparing the spectra of γ-Al_2O_3 before and after CO_2 adsorption, one can see that the OH bands at higher wavenumbers (3785, 3769, and 3748 cm^{-1}) that are assigned as "basic" OH groups are essentially eliminated by interaction with CO_2. A new shoulder at approximately 3610 cm^{-1} appears. To minimize the interference from the OH groups, the IR spectra of the pre-adsorption samples (without the chemisorbed CO_2 surface species) were subtracted from the IR spectra of the corresponding post-adsorption samples. The difference spectra are

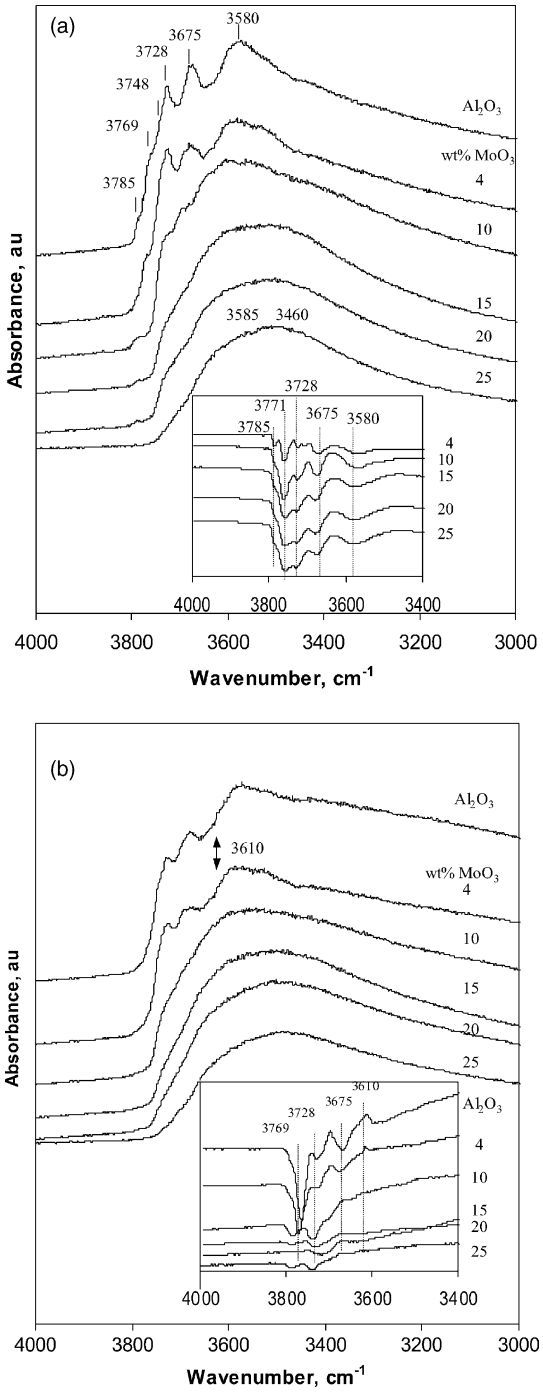

Fig. 3. DRIFT spectra of the hydroxyl region on oxidic MoO_3/Al_2O_3 samples: (a) before CO_2 adsorption, (b) after CO_2 adsorption.

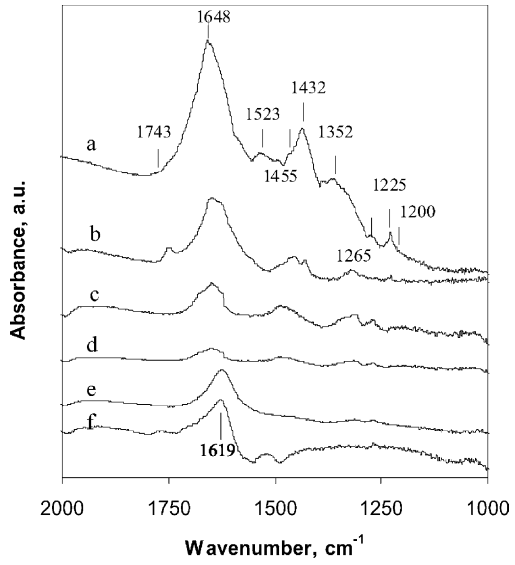

Fig. 4. DRIFT spectra of chemisorbed CO_2 on oxidic MoO_3/Al_2O_3 samples: (a) γ-Al_2O_3, (b) 4% MoO_3/Al_2O_3, (c) 10% MoO_3/Al_2O_3, (d) 15% MoO_3/Al_2O_3, (e) 20% MoO_3/Al_2O_3, (f) 25% MoO_3/Al_2O_3.

presented in the inset. The additional band at 3610 cm^{-1} (see the inset of Fig. 3(b)) is seen more clearly for Al_2O_3 and 4% MoO_3/Al_2O_3 samples. This band can be attributed to the OH stretching mode of bicarbonate species adsorbed on γ-Al_2O_3 [25,26]. Comparing the pre- and post-adsorption spectra, one can see that OH bands at 3785 and 3769 cm^{-1} are completely removed upon CO_2 adsorption. The bands at 3728 and 3675 cm^{-1} are also reduced in intensity significantly. The negative peaks (in inset) that correspond to the loss of OH groups imply that CO_2 preferentially reacts with basic OH groups. The above observations are consistent with earlier reports from the literature [21,22,26]. It should be pointed out that the band at 3785 cm^{-1}, which did not disappear with increasing Mo loadings, have disappeared completely for all samples after CO_2 adsorption (Fig. 3). It is possible that the OH groups that are not accessible to molybdate ions can still interact with CO_2.

Fig. 4 shows the low-frequency region of the IR spectra of adsorbed CO_2 obtained from bare support and oxidized MoO_3/γ-Al_2O_3 samples. The spectrum obtained from the γ-Al_2O_3 surface shows features characteristic of five different groups of chemisorbed CO_2 species reported earlier on metal oxide surfaces [27]: (i) bicarbonate species (3610, 1648, 1445 and 1225 cm^{-1}); (ii) monodenate species (1523 and 1352 cm^{-1}); (iii) bridged species (1743 and 1200 cm^{-1}); (iv) bidentate species (1265 cm^{-1}) and (v) "free" carbonates (1432 cm^{-1}). The IR spectra of the surface species formed upon chemisorption of CO_2 on MoO_3/γ-Al_2O_3 samples show similar features to those observed on bare γ-Al_2O_3 surface, except the band intensities are much lower. It was suggested earlier that the IR bands observed upon chemisorption of CO_2 on MoO_3/γ-Al_2O_3 surfaces result from the interaction of CO_2 with OH groups of exposed alumina surface [26,28,29]. With the increase in MoO_3 loading, the bands from monodenate species and bridged species disappear quickly. A comparison with the hydroxyl region of the corresponding IR spectra may suggest that these species are associated with more basic OH groups on alumina.

If, as proposed by Topsoe and Topsoe [23], the monolayer coverage is governed by the OH group density rather than by the exposed alumina surface area, the IR spectra suggest that monolayer coverage is reached when MoO_3 loading

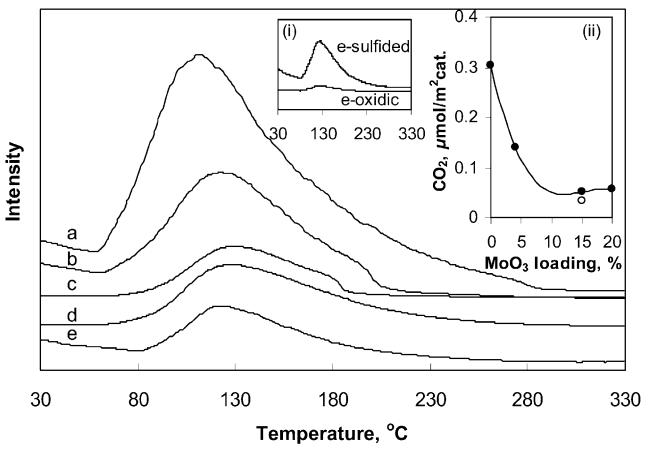

Fig. 5. CO_2 TPD profiles on sulfided samples: (a) Al_2O_3, (b) 4% Mo/Al_2O_3, (c) 15% Mo/Al_2O_3, (d) 20% Mo/Al_2O_3, (e) 3% Ni-15% Mo/Al_2O_3.

level is 15%. The intensities of the bands assigned to the chemisorbed surface CO_2 species for 15% MoO_3/γ-Al_2O_3 are significantly lower than those observed for lower Mo loadings. The fact that these bands do not disappear completely when monolayer coverage is reached can be explained by the presence of OH groups that remained on the surface even at higher Mo loading levels, but disappeared readily upon CO_2 adsorption. A new band at 1619 cm^{-1} appears at MoO_3 loading beyond 15% and the intensity of this band increases sharply with increase in MoO_3 loading. This new band can be assigned to CO_2 species adsorbed on small crystallites of MoO_3 since the bidentate carbonates on the surface of crystalline of MoO_3 appears at 1619 cm^{-1} [22]. These results are consistent with the observations made through XRD and LRS [15].

3.2. Characterization of sulfided catalysts

3.2.1. CO_2 TPD

CO_2 TPD profiles over bare support, mono-, and bi-metallic samples which are sulfided in situ, are shown in Fig. 5. CO_2 is seen to desorb showing a broad temperature maximum in the 80–180 °C range. The amount adsorbed is seen to decrease sharply with MoO_3 loading on Al_2O_3 support up to 15% (see inset (ii) in Fig. 5). The data point that corresponds to the bi-metallic (3% Ni-15% Mo) is also included for comparison (blank point). There is not a significant change with further increases in MoO_3 loading, which is a trend similar to that observed for oxidic samples through IR studies. With NiO addition, adsorbed CO_2 amount on sulfided bi-metallic catalyst somewhat decreases. Sulfided samples have significantly larger CO_2 adsorption capacity compared with oxidic samples (inset (i) in Fig. 5).

3.2.2. DRIFT spectra of CO_2 adsorption on sulfided samples

Fig. 6 shows DRIFT spectra of adsorbed CO_2 on sulfided support, mono-, and bi-metallic samples. DRIFT spectra obtained following CO_2 adsorption exhibit bands similar to those observed for oxidized samples. The major bands observed are 1652, 1439, and 1225 cm^{-1}, which are similar to those observed for oxidized samples. The intensities of adsorbed CO_2 bands are similar for sulfided and unsulfided Al_2O_3 support. However, the intensity of adsorbed CO_2 bands are stronger over the sulfided catalysts compared to the oxidized catalysts. The intensity of the CO_2 adsorption bands over bi-metallic NiMo catalyst, on the other hand, is much lower than that over the mono-metallic Mo catalyst, suggesting that the presence of Ni may be enhancing the dispersion of Mo on the surface. This observation is consistent with our earlier results obtained through TPD, X-ray diffraction, laser Raman spectroscopy and X-ray photoelectron spectroscopy studies [15].

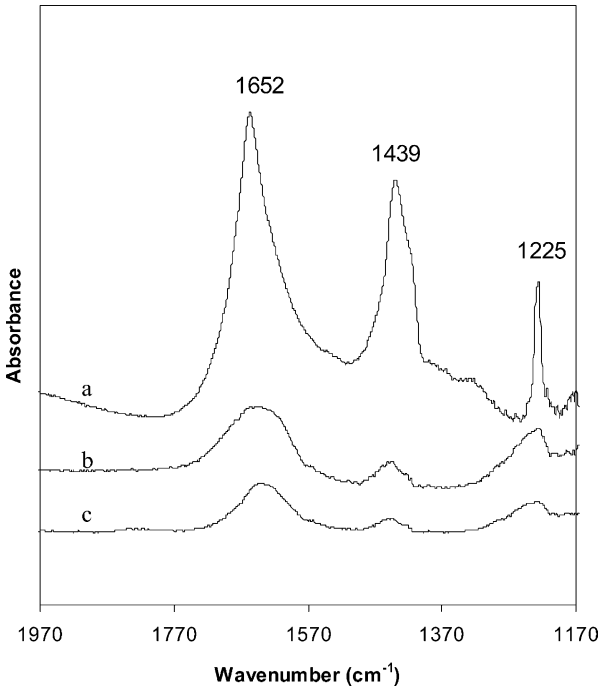

Fig. 6. DRIFT spectra of chemisorbed CO_2 on sulfided samples: (a) Al_2O_3, (b) 15% Mo/Al_2O_3, (c) 3% Ni-15% Mo/Al_2O_3.

As will be discussed in the next articles of this series, CO_2 can be used as a probe molecule for specific sites on the surface and its uptake can be correlated with selectivity trends observed in aldehyde hydrogenation reactions [30]. Since CO_2 adsorption is related to the surface hydroxyl groups, any changes in the surface OH group concentration is likely to affect the product distribution in these reactions.

3.3. Hydrogenation of hexanal

The products observed in hexanal hydrogenation reaction are grouped as hexanol, which is the major product, the lights, and the heavies. Hexanol forms from hydrogenation of the C=O double bond of hexanal. “Lights” refers to products with carbon number lower than that of the feed hexanal, such as paraffins, CO, and/or methanol, which form

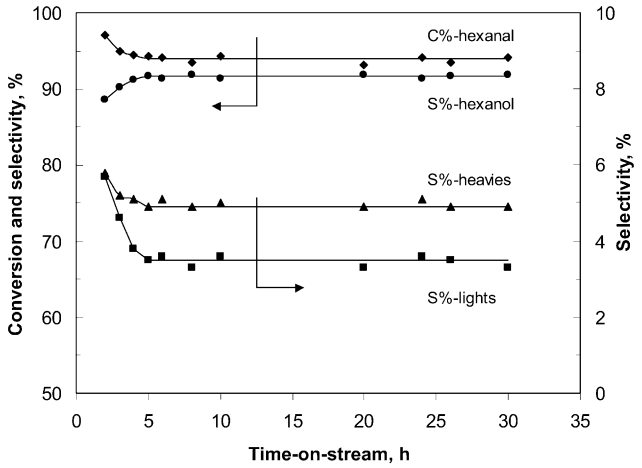

Fig. 7. Performance of sulfided 3% Ni-15% Mo/Al_2O_3 catalyst in hexanal hydrogenation at 180 °C, 1000 psig, and 0.09% hexanal in 250 cm^3/min H_2, 20 m^2 catalyst.

from hydrogenation, decarbonylation, and C–C bond cleavage. "Heavies" refers to products heavier than hexanol, such as dimers, trimers, acetals, and ethers, which result from several side reactions including polymerization, aldol condensation and dehydration. Hydrogenation of hexanal in a blank reactor (without catalyst) showed no detectable reaction. Initial experiments performed to determine the time needed to reach steady state showed that the conversion and selectivity levels remained steady after 5 h (Fig. 7). All of the reaction data presented in this article were collected after steady state was reached.

3.3.1. Hydrogenation of hexanal over sulfided monometallic catalyst

The effect of Mo loading on conversion and product distribution in mono-metallic catalysts is presented in Table 2. The reaction experiments were performed at temperatures ranging from 140 to 180 °C, keeping other reaction parameters constant (pressure = 1000 psig, concentration of hexanal = 0.09 mol%, hydrogen flow rate 250 cm^3 (STP)/min, catalyst loading in the reactor = 25 m^2). It can be seen that conversion of hexanal increases gradually with increasing MoO_3 loading up to 15%. Further increase in the loading shows a slight decrease in conversion. The selectivity to alcohol increases with increasing MoO_3 loading up to 15%, where it reaches a plateau. The selectivity to light products continuously increases with increasing MoO_3 loading. The selectivity to heavy products decreases with increasing MoO_3 loading. No significant changes were observed after the Mo loading level reached 15%. In summary, hydrogenation of hexanal over sulfided monometallic $Mo/\gamma\text{-}Al_2O_3$ catalysts shows optimum performance with 15% MoO_3 loading.

As expected, higher reaction temperature yields higher conversion of hexanal. With increasing temperature, selectivity to hexanol increases, while selectivity to heavies is depressed. Although much smaller than alcohol or heavy selectivities, the selectivity to lights also increases with temperature. The same trend holds for all catalysts.

3.3.2. Hydrogenation of hexanal over sulfided bi-metallic catalyst

Table 3 shows the results of hydrogenation of hexanal over sulfided bi-metallic catalysts where Mo loading is kept constant at 15% MoO_3 and the Ni loading is varied. The reaction runs were performed using the same reaction parameters as mentioned above. It is seen that conversion of hexanal increases with increasing NiO loading up to 5%. Further increase in the addition of NiO induces a slight decrease of conversion. The selectivity to alcohol goes through a maximum with increasing Ni, maximum taking place at 3% NiO. The selectivity to light products continuously increases with increasing NiO addition. Especially with NiO loadings beyond 3%, a significant increase is observed. The selectivity to heavy products first decreases with increasing NiO addition, but levels off at loading levels higher than

Table 2
Variation of hexanal conversion and product selectivity with reaction temperature over sulfided mono-metallic $Mo/\gamma\text{-}Al_2O_3$ catalysts

Catalyst	Temperature (°C)	C (%)	S (%)		
		Hexanal	Hexanol	Lights	Heavies
Sulfided (4% Mo)	140	13.5	29.6	0.4	70.1
	160	29.2	55.9	0.6	43.5
	180	50.3	65.5	2.0	32.5
Sulfided (10% Mo)	140	17.4	57.6	0.6	41.7
	160	39.6	72.4	1.7	26.0
	180	70.2	80.1	2.4	17.5
Sulfided (15% Mo)	140	17.8	66.1	1.5	32.4
	160	44.9	80.8	2.1	17.0
	180	80.1	84.9	2.5	12.6
Sulfided (20% Mo)	140	18.0	63.8	1.3	34.9
	160	43.7	79.9	2.2	17.9
	180	77.0	83.7	2.8	13.5

Table 3
Variation of hexanal conversion and product selectivity with reaction temperature over sulfided bi-metallic $Ni\text{-}Mo/\gamma\text{-}Al_2O_3$ catalysts

Catalyst	Temperature (°C)	C (%)	S (%)		
		Hexanal	Hexanol	Lights	Heavies
Sulfided (1% Ni-15% Mo)	140	21.7	69.1	1.6	29.3
	160	50.3	81.5	2.6	15.9
	180	87.1	86.6	3.0	10.4
Sulfided (3% Ni-15% Mo)	140	22.6	74.4	3.0	22.6
	160	57.3	85.3	3.2	11.5
	180	99.2	87.6	4.1	8.3
Sulfided (5% Ni-15% Mo)	140	25.3	72.8	4.5	22.7
	160	58.2	82.7	5.6	11.7
	180	98.1	87.2	7.1	5.7
Sulfided (7% Ni-15% Mo)	140	24.5	71.9	6.8	21.3
	160	57.2	79.1	9.2	11.7
	180	97.5	86.0	11.0	3.0

Table 4
Effect of H_2O on hexanal hydrogenation over sulfided 3% Ni-15% Mo/γ-Al_2O_3 catalyst

Condition	*C* (%)	*S* (%)		
	Hexanal	Hexanol	Lights	Heavies
Without H_2O	82.8	92.3	1.9	5.8
With H_2O	60.3	98.9	0.9	0.2

3%. A comparison of the yields for hexanal shows that a Mo loading level of 15% and a Ni loading of 3–5% give the optimum catalyst performance. The effect of reaction temperature on conversion and product distribution is similar to that observed for mono-metallic catalysts.

3.4. Effect of H_2O in feed

3.4.1. Hexanal hydrogenation in the presence of H_2O

The effect of H_2O on reaction performance and catalyst properties was studied by introducing H_2O as co-feed. A comparison of conversion and selectivities obtained over sulfided 3% Ni-15% Mo/Al_2O_3 catalyst with and without water is presented in Table 4. The reaction experiments were performed at 160 °C and 1000 psig using hexanal and water concentrations of 0.5 and 0.2%, respectively. The presence of water was seen to suppress the heavy and light product formation and improve the hexanol selectivity. The overall conversion was also suppressed. Effect of water on the long-term performance of the catalyst was examined by keeping the catalyst on-line for 300 h (Fig. 8). The water concentration was kept at a rather high value so that an "accelerated" deactivation effect could be observed. The conversion of hexanal showed some decrease with increasing time on-stream. The selectivity to hexanol, on the other hand, appeared to be relatively stable after a transient period.

3.4.2. Post-reaction TEM/EDX experiments

Fig. 9 shows pre- and post-reaction TEM micrographs of a sulfided 3% Ni-15% Mo/Al_2O_3 catalyst. The dark lines observed in the TEM micrographs are likely to be the edge planes of MoS_2 slabs, as reported earlier in the literature [32], showing primarily a stacking degree of two (Fig. 9(a)). The slabs that are parallel to the surface of the oxide support would not show on these images, so these micrographs do not necessarily provide conclusive information about the orientation of MoS_2 slabs. However, they are consistent with earlier studies that report a single layer thickness of about 0.6 nm and a typical length of about 2.5 nm for MoS_2 slabs. They are also seen to "bend" when the slab length becomes longer. The TEM images taken after hexanal hydrogenation reaction in the presence of water show a higher density of these dark lines, with a higher stacking order, suggesting a possible rearrangement on the surface due to reaction (Fig. 9(b)). However, since the number of TEM images is not large enough to be statistically significant, it is difficult to draw definitive conclusions

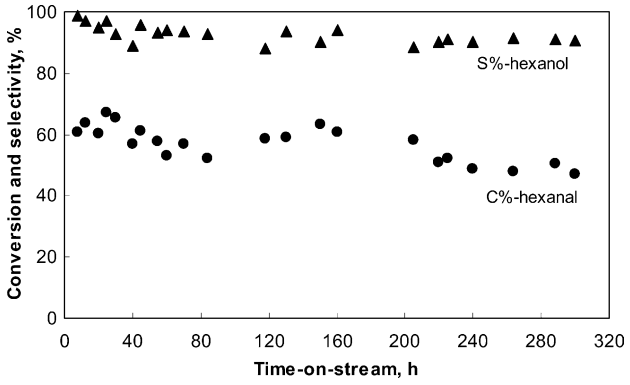

Fig. 8. Change of activity and selectivity with time on-stream in hexanal hydrogenation in the presence of H_2O over sulfided 3% Ni-15% Mo/Al_2O_3 catalyst.

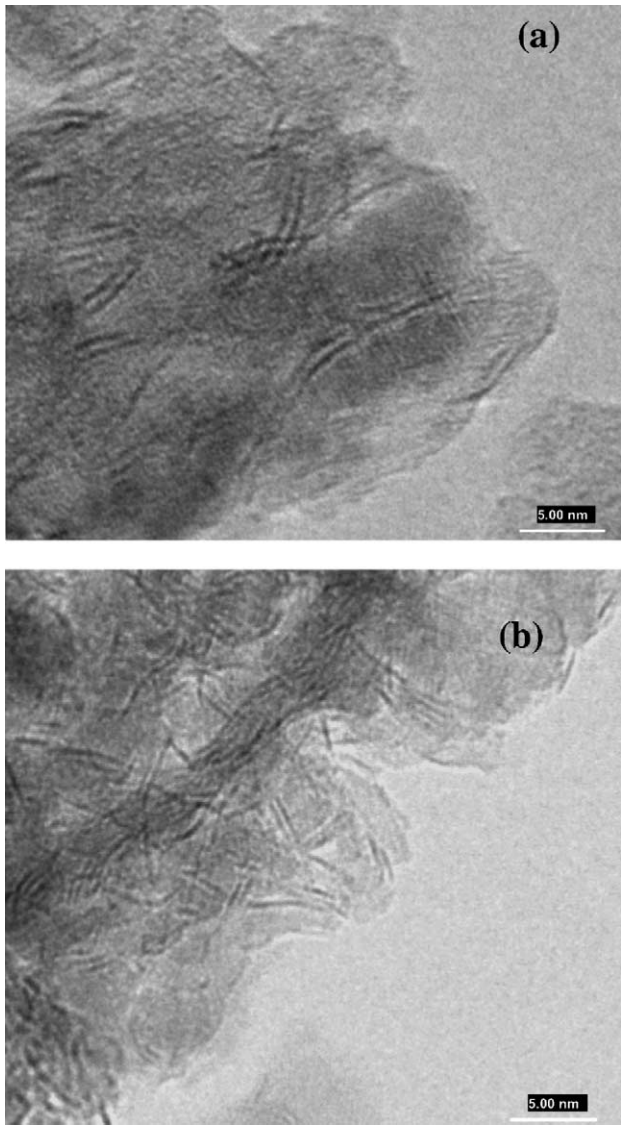

Fig. 9. TEM micrographs of sulfided 3% Ni-15% Mo/Al_2O_3 catalyst: (a) pre-reaction, (b) post-reaction with H_2O.

Table 5
Atomic ratios of major elements on pre- and post-reaction sulfided 3% Ni-15% Mo/γ-Al_2O_3 catalyst from XPS and TEM/EDX measurements

Atomic ratio	Pre-reaction		Post-reaction	
	XPS	EDX	XPS	EDX
Ni/Al	0.04	0.03	0.01	0.02
Mo/Al	0.10	0.07	0.05	0.06
O/Al	1.45	1.93	1.86	1.95
S/Al	0.26	0.18	0.12	0.16
C/Al	0.86		2.36	
S/Mo	2.63	2.56	2.38	2.55
Ni/Mo	0.40	0.43	0.20	0.42
Mo^{6+} (%)	6		13	
Mo^{5+} (%)	–		20	
Mo^{4+} (%)	94		67	

about the surface orientation of the slabs based on the TEM data.

EDX analysis results are summarized in Table 5. For the pre-reaction catalyst, EDX data show that average Ni/Mo ratio (0.43) is close to the theoretical value (0.40). S/Mo ratio is 2.56, which could indicate the presence of Ni sulfide species. Comparing post-reaction catalyst with pre-reaction catalyst, EDX results show no significant difference in average elemental ratios.

3.4.3. Post-reaction XPS experiments

The X-ray photoelectron spectra of the bare γ-Al_2O_3 support were taken before and after sulfidation (not shown). Under the high vacuum operating conditions of XPS measurement (10^{-9} Torr), sulfur was not detected after sulfidation, indicating that there is no bonding between pure alumina and sulfur.

Fig. 10 presents representative spectral regions for individual elements over sulfided 3% Ni-15% Mo/Al_2O_3 catalyst before and after reaction in the presence of water. The atomic ratios of major elements on pre- and post-reaction sulfided 3% Ni-15% Mo/Al_2O_3 catalysts obtained through XPS are listed in Table 5 combined with the results from TEM/EDX experiments. The calculation was based on the integrated peak intensities of Ni 2p3/2, Mo 3d5/2, S 2p3/2, Al 2p, and C 1s corrected by the atomic sensitivity factors. C 1s spectrum (not shown) for the post-reaction sample showed a much higher intensity compared to the pre-reaction sample. This is likely to be due to deposition of carbonaceous species. A pronounced increase in atomic ratio of C/Al for post-reaction catalyst was also observed (Table 5).

In Mo 3d–S 2s region for pre-reaction catalyst, the peaks are attributed to Mo(IV) species (ca. 229 and 232 eV for the $3d_{5/2}$ and $3d_{3/2}$, respectively) and S^{2-} species (226 eV for the 2s). However, deconvoluting spectra by Gaussian–Lorentzian curve-fitting method using the constraints of having 3.15 eV spin-orbit splitting of Mo 3d peak, the area ratio of Mo $3d_{5/2}$ to Mo $3d_{3/2}$ being constant at 1.5 and keeping the full width at half maximum (FWHM) of Mo $3d_{5/2}$ and Mo $3d3_{/2}$ peaks constant, showed that there was a small amount of Mo(VI) present. Quantification results show about 6% Mo being in Mo(VI) state, which should correspond to Mo atoms in a strong interaction with the support [33,34]. Sulfidation of those Mo atoms occur only at temperatures higher than the one used in this process. The percentage of Mo(IV) (94%) after sulfidation lies in the range of 72–100% reported by Portela et al. [35]. The Mo 3d–S 2s region for the post-reaction catalyst is very different from that for pre-reaction catalyst. In addition to the peak intensities being lower due to deposition of carbonaceous species, the peaks are much broader than those for pre-reaction catalyst and shoulders appear on the peaks. Deconvolution results show a distribution of Mo species among three different oxidation states (67% Mo(IV), 20% Mo(V), and 13% Mo(VI)). Surface atomic ratio of O/Al increased after reaction from 1.45 to 1.86 (Table 5), which indicates MoS_2 species being oxidized by H_2O or other oxygen containing components under reaction conditions. The oxidation of active phases by oxygen-containing substances and water during hydrotreating of low sulfur content feeds as a probable cause of catalyst deactivation was reported in the literature [36–40].

The Ni 2p signal is relatively weaker compared with other elements. Spectra for pre-reaction catalyst show clearly $2p_{3/2}$ and $2p_{1/2}$ peaks at ca. 853 and 870 eV, which correspond to the Ni in Ni-Mo-S structure [15]. The spectra for post-reaction catalyst showed a much weaker signal for Ni species. Although a loss of signal from the surface due to its "rearrangement" as shown by the TEM images remains a possibility, the loss of signal could also be due to deposition of carbon species on the surface. Atomic ratio of Ni/Mo from XPS measurement is lower for post-reaction catalyst than for pre-reaction catalyst, while they are very similar from EDX analysis, suggesting that observed signal loss is specific to the surface. The fact that Ni signal appears to be lost preferentially suggests that deposition of C-species occur more selectively over the Ni sites.

Spectrum of Al 2p region for post-reaction catalyst shows a broad peak and a shoulder at the higher binding energy side. The shoulder can be assigned to boehmite species from the partial crystallization of γ-Al_2O_3 support after hydrogenation of hexanal for 300 h reaction in the presence of H_2O. This observation is consistent with earlier findings from the literature, which reported γ-alumina being metastable under hydrothermal conditions and transforming into beohmite in the temperature range of 140–380 °C [41,42].

The S 2p region of the spectrum for the post-reaction catalyst is very different from the pre-reaction one. In addition to intensities being lower mainly due to carbon deposition, peaks are also much broader at the higher binding energy side. Considering two possible sulfur species for the post-reaction catalyst when deconvoluting the spectra, two different binding energies emerge for the S species, one with $2p_{3/2}$ at 162 eV due to S in MoS_2 or NiS phases, and a second one with $2p_{3/2}$ at 164 eV. This second binding

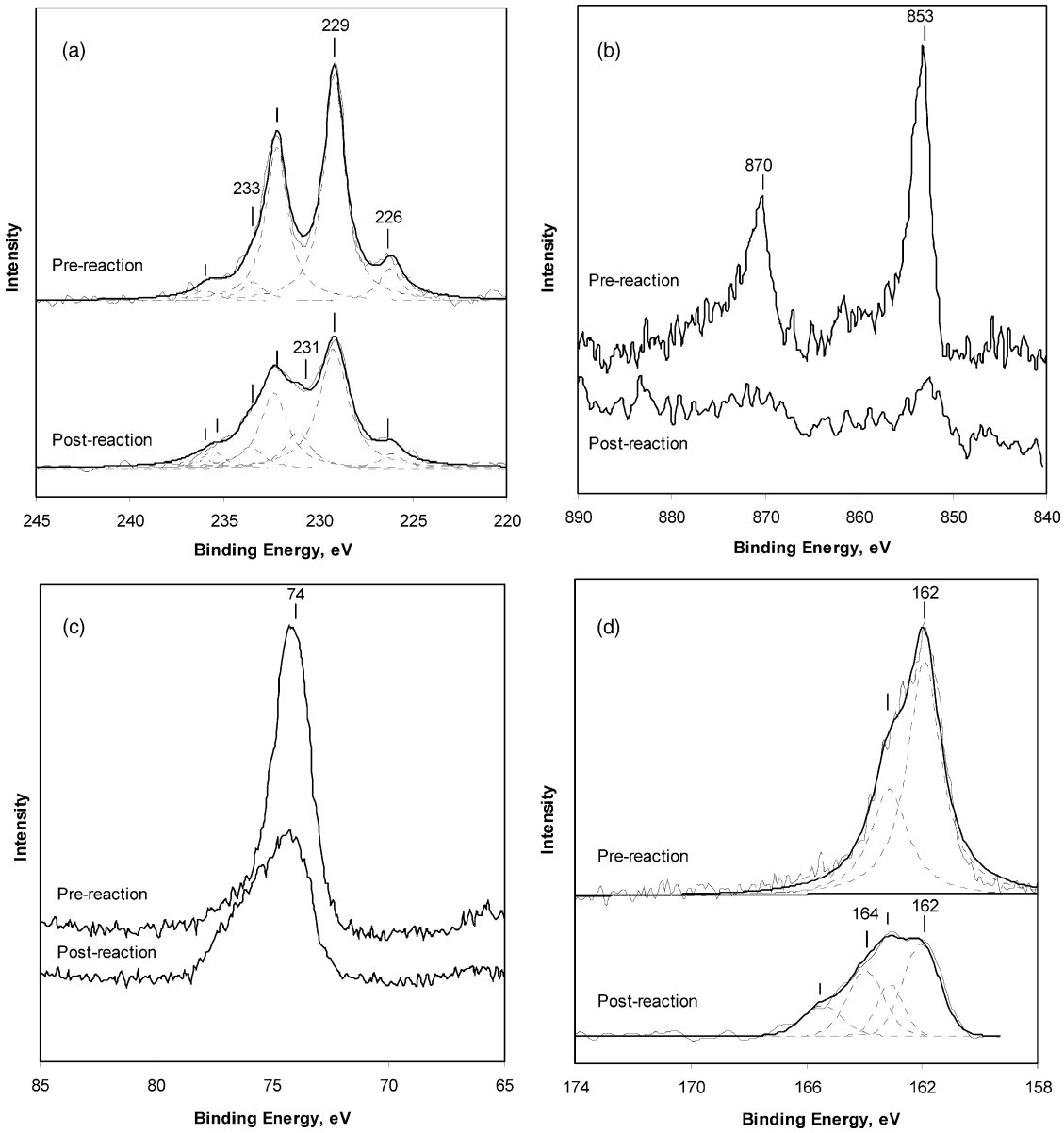

Fig. 10. Pre- and post-reaction X-ray photoelectron spectra of sulfided 3% Ni-15% Mo/Al_2O_3 catalyst: (a) Mo 3d–S 2s region, (b) Ni 2p region, (c) Al 2p region, (d) S 2p region.

energy can be assigned as to sulfur in CS_2 formed from deposition of carbonaceous species.

4. Summary

Studies on hydrogenation of hexanal over sulfided $Ni\text{-}Mo/Al_2O_3$ catalysts have shown a composition of 15% MoO_3 and 3–5% NiO loading to be optimum for highest hexanol selectivity. CO_2 can be used as a probe molecule for quantification of the OH groups on the bare alumina surface, which in turn, can correlate with the yield of heavy products. A monolayer coverage of Mo is essential for minimizing the formation of "heavy" products. This loading level is shown to correspond to a minimum in CO_2 uptake as well as the lowest hydroxyl group concentration on the surface. The presence of H_2O in the feed suppresses the heavy product formation, possibly by passivating the OH sites. Post-reaction characterization following exposure to H_2O showed Mo to be in three different oxidation states (IV, V, VI), suggesting partial oxidation of the surface. There was also a decrease in surface Ni concentration after 300 h of time on-stream. Selective coverage of Ni sites with carbonaceous species or a "rearrangement" of Ni on the surface in the presence of H_2O remain as possibilities. A more detailed discussion of the reaction networks involved in aldehyde hydrogenation and the nature of active sites is presented in the next articles of this series [30,31].

References

[1] G.C.A. Schuit, B.C. Gates, AIChE J. 19 (1973) 417.
[2] P. Grange, Catal. Rev.-Sci. Eng. 21 (1980) 135.
[3] H. Topsoe, B.S. Clausen, Catal. Rev.-Sci. Eng. 26 (1984) 395.
[4] R. Prins, V.H.J. de Beer, G.A. Somorjai, Catal. Rev.-Sci. Eng. 31 (1989) 1.
[5] R.R. Chianelli, M. Daage, M.J. Ledoux, Adv. Catal. 40 (1994) 177.
[6] H. Topsoe, B.S. Clausen, F. Massoth, in: J.R. Anderson, M. Boudart (Eds.), Science and Technology, vol. 11, Springer, Berlin, 1996.
[7] D.D. Whitehurst, T. Isoda, I. Mochida, Adv. Catal. 42 (1998) 345.
[8] H. Topsoe, B.S. Clausen, R. Candia, C. Wivel, S. Morup, J. Catal. 68 (1981) 433.
[9] C. Wivel, R. Candia, B.S. Clausen, S. Morup, H. Topsoe, J. Catal. 87 (1984) 497.
[10] H. Topsoe, B.S. Clausen, Appl. Catal. 25 (1986) 273.
[11] J.J. MeKetta, W.A. Cunningham, Encyclopedia of Chemical Processing and Design, vol. 33, Marcel Dekker, Inc., New York, 1990, p. 46.
[12] P. Grange, Catal. Rev.-Sci. Eng. 21 (1980) 135.
[13] J. Laine, F. Severino, R. Golding, J. Chem. Technol. Biotechnol. A 34 (1984) 387.
[14] U.S. Ozkan, S. Ni, L. Zhang, E. Moctezuma, Energy and Fuels 8 (1994) 249.
[15] U.S. Ozkan, L. Zhang, S. Ni, E. Moctezuma, J. Catal. 148 (1994) 181.
[16] U.S. Ozkan, Y. Cai, M.W. Kumthekar, L. Zhang, J. Catal. 142 (1993) 182.
[17] R.A. Madeley, S.E. Wanke, Appl. Catal. 39 (1988) 295.
[18] J.L. Brito, J. Laine, Appl. Catal. 72 (1991) L13.
[19] P. Dufresne, E. Payen, J. Grimblot, J.P. Bonnelle, J. Phys. Chem. 85 (1981) 2344.
[20] H. Knozinger, P. Ratnasamy, Catal. Rev.-Sci. Eng. 17 (1978) 31.
[21] Y. Okamoto, T. Imanaka, J. Phys. Chem. 92 (1988) 7102.
[22] A.M. Turek, I.E. Wachs, J. Phys. Chem. 96 (1992) 5000.
[23] N.Y. Topsoe, H. Topsoe, J. Catal. 139 (1993) 631.
[24] J. Reardon, A.K. Datye, A. Sault, J. Catal. 173 (1998) 145.
[25] N.D. Parkyns, in: W.M.H. Sachtler, G.C.A. Schutt, P. Zwietering (Eds.), Proceedings of the Third International Congress on Catalysis, vol. II, Amsterdam, 1964, North-Holland, Amsterdam, 1965, p. 914; N.D. Parkyns, J. Chem. Soc. A (1969) 410.
[26] K. Segawa, W.K. Hall, J. Catal. 77 (1982) 221.
[27] V.F. Kiselev, O.V. Krylov, in: G. Ertl, R. Gomer (Eds.), Adsorption and Catalysis on Transition Metals and their Oxides, vol. 9, Springer Series in Surface Sciences, Springer-Verlag, Berlin, 1989.
[28] J.A.R. Van Veen, P.A.J.M. Hendiks, Polyhydron. 5 (1986) 75.
[29] F.M. Mulcahy, M.J. Fay, A. Proctor, M. Houalla, D.M. Hercules, J. Catal. 124 (1989) 23.
[30] X. Wang, R. Saleh, U.S. Ozkan, J. Catal., submitted for publication.
[31] X. Wang, U.S. Ozkan, Appl. Catal., submitted for publication.
[32] E.J.M. Hensen, P.J. Kooyman, Y. van der Meer, A.M. van der Kraan, V.H.J. de Beer, J.A.R. van Veer, R.A. van der Santen, J. Catal. 199 (2001) 224.
[33] D.S. Zingg, L.E. Makovsky, R.E. Tischer, F.R. Brown, D.M. Hercules, J. Phys. Chem. 84 (1980) 2898.
[34] C.P. Li, D.M. Hercules, J. Phys. Chem. 88 (1984) 456.
[35] L. Portela, P. Grange, B. Delmon, J. Catal. 156 (1995) 243.
[36] E. Furimsky, Ind. Eng. Chem. Prod. Res. Dev. 22 (1983) 31.
[37] Y. Yoshimura, H. Yokokawa, T. Sato, H. Shimada, N. Matsubayashi, A. Nishijima, Appl. Catal. 73 (1991) 39.
[38] Y. Yoshimura, T. Sato, H. Shimada, N. Matsubayashi, A. Nishijima, Appl. Catal. 73 (1991) 55.
[39] E. Lanurent, B. Delmon, Stud. Surf. Sci. Catal. 88 (1994) 459.
[40] E. Lanurent, B. Delmon, Appl. Catal. 109 (1994) 97.
[41] E. Lauren, B. Delmon, Stud. Surf. Sci. Catal. 88 (1994) 459.
[42] G. Ervin, E.F. Osborn, J. Geol. 59 (1950) 381.